Deep Mining 2024 – P Andrieux & D Cumming-Potvin (eds)

doi:10.36487/ACG_repo/2465_46

Enhancing the calibration of elastic numerical models through stress measurements and observations of stress-induced overbreak

Gerrit Kotze [a,*], Daniel Santos De Santana [b], Lucas Renan Mendes Machado [b], Quintin Grix [a]

[a] *Open House Management Solutions, South Africa*

[b] *Ero Copper Corporation, Brazil*

Abstract

In deep mines, where high stress conditions can prevail, geotechnical engineers are required to conduct excavation stability assessments and predict excavation damage proactively. The geotechnical engineer usually undertakes a numerical modelling assessment that aims to quantify the causality between mining sequence, layout and damage.

The reliability and value offering of an uncalibrated numerical model are probably similar to the reliability of parametric or sensitivity studies. It is therefore prudent to quantify the pre-mining stress state and to consider the rock mass responses with a view to enhancing the reliability of model results. Examples of responses include seismic event locations and source parameters, instrumentation data, time-dependent deformation of rock, damage in tunnels or pillars, and stress-induced sloughing.

Calibration of elastic models is based on the notion that excess stress is a direct predictor of expected plastic strain. The model calibration process considers the stress state at damage locations in a mine. The stress state can be described by pairs of major and minor principal stresses collected from the corresponding damage locations in the numerical models. To obtain a strength envelope, a curve is fitted through the pairs of data. A manual process of data appreciation is followed, where the fitted curves and interpretation of data are considered with a view to providing a simple criterion for predicting damage.

At Caraiba mine in Brazil, an initial calibration was done using cavity mine surveys and the historically accepted stress tensor. Subsequently the model input parameters were updated using actual stress measurements and then followed by an update of the initial calibration. Elastic models are quick to set up and the observational method of model calibration is relatively simple to execute. This methodology is attractive to geotechnical engineers since they have to collect rock mass response data routinely and they have limited time to conduct numerical modelling.

Keywords: *stress-induced overbreak, model calibration, damage observations, elastic modelling*

1 Introduction

1.1 The value and purpose of ongoing data collection

Geotechnical engineers are expected to conduct excavation stability assessments, and advise mine owners on the potential for damage, in a proactive manner. In some geotechnical settings the stress state, and for others, structural domains, control/s the ground stability. In all cases, data collection informs both the interventions that reduce risk and the inputs to mining geotechnical engineering design. One of the main

* Corresponding author. Email address: gerrit.kotze@ohms.co.za

functions of the geotechnical engineering department at a mine is to make the connection between models, design principles, geotechnical data and observations of rock mass responses.

During the early operational stages of a mine, the data collection process is often neglected because of the focus on operational requirements. This is especially the case if the rock mass is not yet responding in an unpredictable or unstable manner. Neglecting geotechnical data collection is not a sustainable practice because as construction progresses, mines could experience potentially damaging rock mass responses, e.g. seismic activity, overstressed pillars, scaling of orepasses, tunnel damage, squeezing behaviour or unplanned stress-induced overbreak around stopes. A routine data collection program is required from the onset to establish a baseline of rock mass response.

Table 1 describes the level of effort required for numerical models in the context of the availability of data for calibration. Tick marks indicate the strengths and crosses indicate weaknesses. The so-called Level 1 models are based on non-quantitative inputs and are not calibrated, possibly due to lack of effort or absence of data. Level 1 damage predictions are expected to be vague and ambiguous. As cost-benefits and trade-offs are not reliable when using Level 1 models, the value added to an operational process is limited. Level 1 model reliability would likely be on par with models developed for sensitivity analysis or scoping level studies. In contrast, Level 4 models add value to operational processes because a connection was made between model results and the collected geotechnical data.

Table 1 Level 1 to Level 4 numerical modelling efforts (Wiles 2024b)

Level of modelling effort			
Level 1	**Level 2**	**Level 3**	**Level 4**
Parametric/demonstration modelling × No σ^f, *UCS*, *q*, *s* or *minimisation** ✓ Demonstrate realistic behaviour × Little in the way of real design numbers ✓ Modelling can be completed inexpensively with little or no site-specific information × Predictions are vague and ambiguous × Impossible to make informed cost-benefit trade-offs	Qualitative modelling ✓ With σ^f, *UCS* and *q* × No *s* or *minimisation* ✓ Applied in feasibility studies/greenfield sites. ✓ Inexpensive since no back-analyses required × Predictions are relatively vague and ambiguous × *s* is quite large or unknown × Poorly optimised designs	Quantitative modelling ✓ With σ^f, *UCS, q* and *s* × No *minimisation* ✓ Predictions are informing a specific rock *response* to be expected ✓ *s* is determined as part of the back-analysis ✓ Assess safety and make cost-benefit trade-offs × Cannot be applied in greenfield sites × Increasingly more expensive	Optimised quantitative modelling. ✓ With σ^f, *UCS, q, s* and *minimisation* ✓ Best reliability – well-optimised designs × Most expensive considered here and can require a large amount of engineering effort × Cost of the extra modelling effort required to minimise *s* can be traded off against options for mine layouts but not being done

*Where σ^f = far field stress; UCS = uniaxial compressive stress; q = slope of strength envelope; s = statistical variance

1.2 Elastic numerical modelling, strength envelope for damage categories and model calibration

Numerical modelling is used on mines for back-analyses of rock mass behaviour and to predict 'damage' ('overstressed' rock). Damage may have qualitative descriptions but is quantified using principal stresses that are obtained from numerical models. A non-exhaustive list of damage occurrences, including some caveats, is found in Table 2. The 'survivalist' bias must be avoided and, to achieve a robust calibration, all the response classes from a type of damage occurrence should be considered, e.g. 'good', 'average' and 'adverse' ground conditions in tunnels.

Table 2 Non-exhaustive list of damage occurrences, damage classes and some caveats

Type of occurrence	Damage class examples	Some caveats
Overbreak (stress-induced sloughing) around open stopes	Depth of overbreak. Overbreak relative to extraction sequence, viz. primary, secondary, tertiary or first lift, second lift, etc. Isolated stope, secondary operation. Overbreak per geo domain	Yielded zone can extend beyond a cavity mine survey scan. Damaged rock could be confined by arching effects and interpreted as undamaged rock. Anisotropy could influence effectiveness of assessment
Scaling in orepasses and borehole breakout (dog-earing)	Depth of impression Frequency of cracks	Orientation of stress-induced impressions used to infer orientation of field stress. Anisotropy could influence effectiveness of assessment
Seismicity	Slip or burst events, abutment failures, rock mass failures Fault slip solutions from moment-tensor solution to determine likely structure involved in slip	Velocity model could cause bias in event location. Events could locate in a low-stress zone in the model while events are associated with highly stressed rock
Damage in tunnels (Gothic arching)	Good, average and adverse conditions	Time dependency, causality with extraction sequence and anisotropy could influence effectiveness of assessment

Calibration is primarily concerned with making connections between model results and damage observations. Calibration of numerical models can be achieved by studying the causality between damage, field stress and layout, while prediction can be achieved by extrapolating the calibration. Calibration of elastic models is based on the notion that excess stress is a direct predictor of expected plastic strain. The stress state can be described by pairs of major and minor principal stresses collected from the corresponding damage locations in the numerical models. To obtain a strength envelope a curve is fitted through the pairs of data that can be connected to a specific type of rock mass response. As a first pass the reliability of the elastic model calibration can be improved by adding more examples of the same category of damage. According to the experience of the authors, which is aligned with work by, for example, Wiles (2005) and Harr (1978), the reliability of the calibrated strength enveloped obtained from elastic models typically compares to the errors arising from laboratory testing of samples. This approach to calibration is certainly not a novel approach and has been described in a quantitative manner by Wiles (2005).

One of the primary advantages to elastic modelling is that strength parameters are not required as input parameters for an excess stress analysis. Only three primary input parameters, namely the three pre-mining principal stress components, are required. Plastic models necessitate calibration of at least nine input parameters, hence elastic modelling provides a simplified approach to back-analyses.

The shortcoming of elastic modelling is that stresses are not re-distributed and part of the simulated layout could potentially become overstressed at unrealistic levels. However, if there is not a significant amount of stress redistribution occurring in reality, it is not a limitation. If a significant amount of stress redistribution is required for a specific scenario then plastic modelling-based approaches may improve confidence in the models results, but they require additional effort to calibrate the additional input parameters.

Figure 1 (Wiles 2024b) shows that the case for elastic modelling can be appreciated by considering the relationships between the strength envelope coupled to a damage category, the loading path to failure and the stress-strain curve for elastic rock mass assessments. The scenario in Figure 1 a is a simplified load path applicable to, for example, pillar failure, where σ_1 is increasing while σ_3 is approximately constant. The loading path depicted in Figure 1 b is representative of another type of damage, namely abutment failure, where deviatoric stress ($\sigma_1 - \sigma_3$) is the damaging stress.

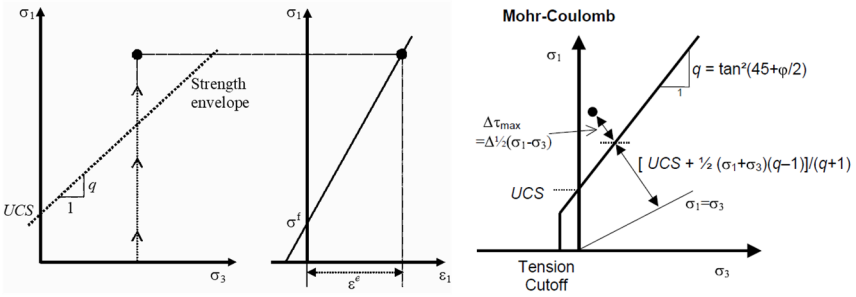

(a) (b)

Figure 1 Loading paths and strength envelope for elastic modelling: (a) σ_1 varies; (b) σ_1 and σ_3 varies

1.3 Stress measurements

The magnitude and orientation of pre-mining stresses are critical input parameters for all numerical modelling codes. Too often the stress tensor is assumed to be hydrostatic or is informed by a regional stress model, which results in a Level 1 to Level 2 model reliability. Such vague assumptions could lead to an invalid interpretation of model results and either a too conservative or too liberal mine design.

1.4 Geotechnical background of Caraiba operations

The cases discussed in this paper were selected from Canadian group Ero Copper Corporation's Caraiba copper ore mine, located 385 km from the Bahia state capital in northeastern Brazil (Ero Copper Corporation 2022). An initial open cut operation was developed into the Pilar underground mine, which is currently yielding production at 6,000 t per day. The deposit lies within the Curaça Valley mafic-ultramafic complex in the northern portion of the São Francisco Craton. The host rock comprises gneiss (UCS = 160 MPa, Young's modulus = 69 GPa) pierced by copper-bearing mafic-ultramafic intrusions, represented by gabbroic rocks and pyroxenite (UCS = 150 MPa, Young's modulus = 89 GPa). Except for fault zones, the rock mass is presenting brittle failure type responses that could manifest as strain or rockbursts. The steeply dipping north–south striking orebodies are pierced by west- and east-dipping fault zones, which are associated with an intensely jointed rock mass. Initially the mining method involved sublevel open stopes with dimensions of 95 m height, 35 m width and 80 m length. Sill pillars averaging 20 m in thickness were part of this layout, and used up to a depth of 550 m. The vertical retreat mining method with paste or waste rockfill was introduced to manage dilution and the stope height was adjusted from 26 to 35 m. As mining is progressing beyond 1,400 m, the primary-secondary stope, bottom-up and centre-out mining layout is being replaced by longitudinal or transverse stoping, depending on the width of the orebody.

In 2021 a Map3D model was constructed for Caraiba mine and it is being updated on an ongoing basis. Initially the objective of the model was to assess geotechnical risk of the life of mine (LOM) plan. It was realised early on that the models do not add significant value to the planning process without a connection being made between the observed unplanned overbreak and the potential for overstressing of rock. A methodology was therefore developed and is described in the following section.

2 Methodology

The model calibration methodology developed at Caraiba mine is applicable to a wide range of geotechnical environments. Numerical models are supposed to be a simplification of reality. At a mining operation the methods that make connections between data and model results must be practical and easy to implement on a routine basis. The Caraiba methodology was inspired by Occam's razor (Simms 2024), which suggests an approach to problem-solving that involves the least number of factors. Also implied is that if there are two competing ideas to explain the same phenomenon, one should prefer the simpler one: initially, use elastic models, damage observations and regression analyses, and later, plastic modelling.

2.1 Workflow for model calibration

Figure 2 shows a block representation of workflow involved in the model calibration process, which is discussed in detail in this section. One of the objectives of the LOM assessment was to proactively determine and predict stress-induced sloughing. Hence there was a focus on calibrating models of the LOM stoping layout using overbreak events from the past.

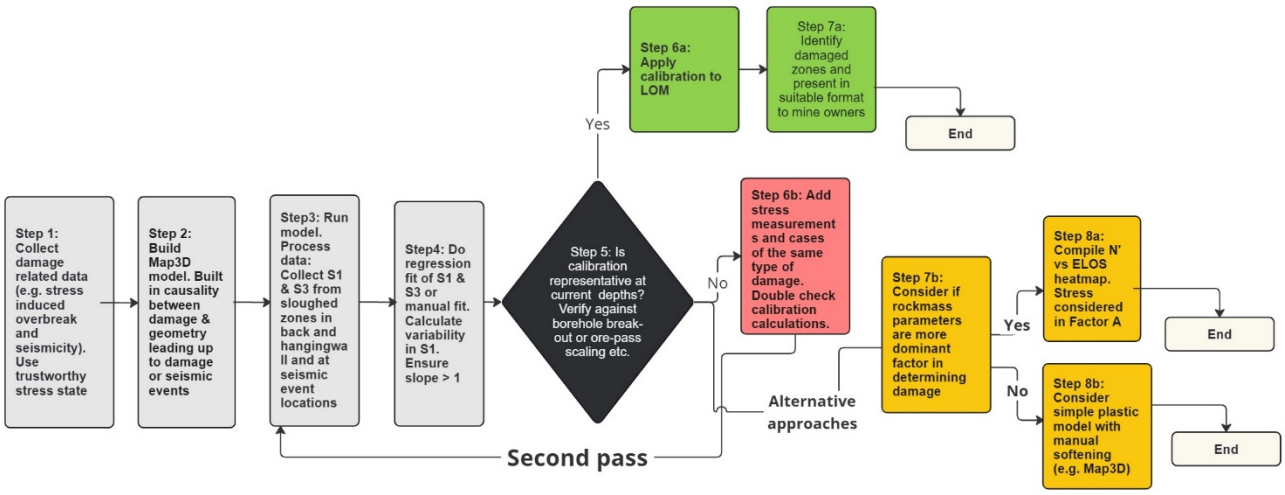

Figure 2 Workflow of the model calibration process

Stope reconciliation reports are used to inform the stopes thought to experience stress-induced (>0.5 m) sloughing. Stopes that sloughed due to execution errors during rock breaking, or due to kinematic or geological factors, were not considered for calibrating models. Although anecdotal, the reported audible seismic emissions were considered for informing stress-induced overbreak in some cases.

A mine-wide numerical model, with a mining sequence that includes the step at which sloughing occurred, was used. Initially the stress tensor specified in the ground control management document was used. The σ_1 and σ_3 values were collected (Figure 3) from damage locations in the converged numerical models.

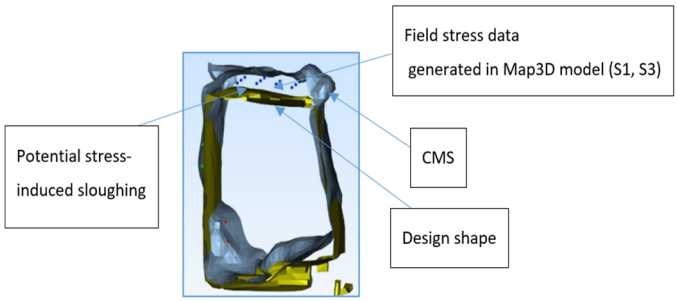

Figure 3 Example showing the field points at which data were collected in the sloughed zone. Note: CMS = cavity mine surveys

To consider reliability statistics at least 30 different cases should be analysed per damage category, but this many cases were not available at the time of the analyses. A regression line was fitted through clusters of σ_1 and σ_3 values. Upon inspecting the data a few trends were identified, namely that the clusters of data could be connected to depth of overbreak and according to the stage of extraction, e.g. isolated primary stope, primary stope against abutment, tertiary stope, etc. A regressing analysis was conducted using Microsoft Excel, and considered the following rock mechanics-based logic:

- Brittle failure (stress-induced fracturing (Martin 1997; Martin & Maybee 2000) initiates at:

$$\sigma_1 - \sigma_3 > R \times UCS \quad (1)$$

where $0.3 < R < 0.5$.

- Crack initiation (Castro 1996) begins at:

$$\sigma_1 - \sigma_3 > 0.4 \times UCS \quad (2)$$

- The threshold ranges of onset of brittle failure mechanisms can be represented by a simple linear relationship that expresses the strength of rock (Diederichs et al. 2004; Wiles 2024a):

$$\sigma_1 = B \times \sigma_c + A \times \sigma_3 \quad (3)$$

where for all three equations:

σ_1 = major principal stress (MPa).

σ_3 = minor principal stress (MPa).

UCS or σ_c = uniaxial compressive strength (MPa)

scaling factor B = $0.3 < B < 0.5$.

slope A = $1 < A < 1.5$.

From the best-fit trend line the following can be determined:

- $B \times \sigma_c$ is the intercept of the graph and represents the strength of the rock mass (UCS_{RM}).
- The internal friction angle (φ) of the rock mass is calculated using $Slope\ A = \frac{(1+\sin\varphi)}{(1-\sin\varphi)} \geq 1$ as otherwise the internal friction angle would be negative.
- $c = \frac{UCS_{RM}}{2\times\sqrt{A}}$ gives an indication of the cohesion of the rock mass for a specific damage category.

Based on the trend analyses, the engineer must exercise judgement (step 5 in Figure 2) to ascertain the range of mining depths where the analyses remain valid. Step 5 allows for testing the limits of the analyses by verifying the results using other damage classes such as borehole breakouts, or scaling in orepasses. To achieve this, field points was inserted into the Map3D model at the validation points. The validation points were located at a similar mining depth to where the stress-induced overbreak occurred.

Following verification the results can be applied to the LOM plan to predict other locations of damage or, if an unsatisfactory calibration was obtained, a second pass of the process must be undertaken using additional case studies. The Caraiba mine instead opted to update the stress model by conducting stress measurements covering a greater range of depths.

While not applicable at the current greater mining depths at the Caraiba operations, if the second pass also fails to produce satisfactory model calibration results it becomes crucial to explore alternative approaches as outlined in steps 7b, 8a and 8b. In certain scenarios a combination of overstressing and variable rock mass quality may jointly contribute to damage. To address this further a heatmap could be created with a modified stability number, N', to express the geotechnical domains for overbreak.

As a final recourse, running a plastic Map3D model with manual softening can be attempted. Discussion of this approach is outside the scope of this paper.

3 Data

The data that were used in the workflow is described in this section.

3.1 Initial stress model

Figure 4 contains the components of the stress model pre-2023 (pre-Y2023) that was used as the initial Map3D model inputs. The directions of the stress components were inferred from engineering judgement. The pre-Y2023 stress model was used for a number of years and it was thought that this model should be validated as it was established when mining occurred at shallower depths. Nevertheless the model was regarded as a reasonable starting point for analysing unplanned stress-induced overbreak.

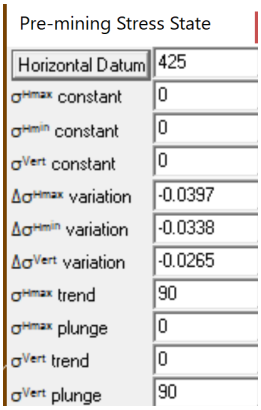

Figure 4 Stress model in use before 2023

3.2 Stress measurements (in 2023)

During 2023 the mine embarked on a stress measurement program (referred to as Y2023) to improve the confidence in design calculations and to verify the pre-Y2023 stress model. Three stress measurement sites were identified and Figure 5 reveals a well-distributed selection of sites thought to be outside the influence of excavations:

- Site 1 (229 m below surface) is between two major ore-parallel faults and is positioned between the open pit and underground mining areas.
- Site 2 (672 m below surface) is located in the footwall of the faults.
- Site 3 (1,449 m below surface) is situated in the deeper part of the mine.

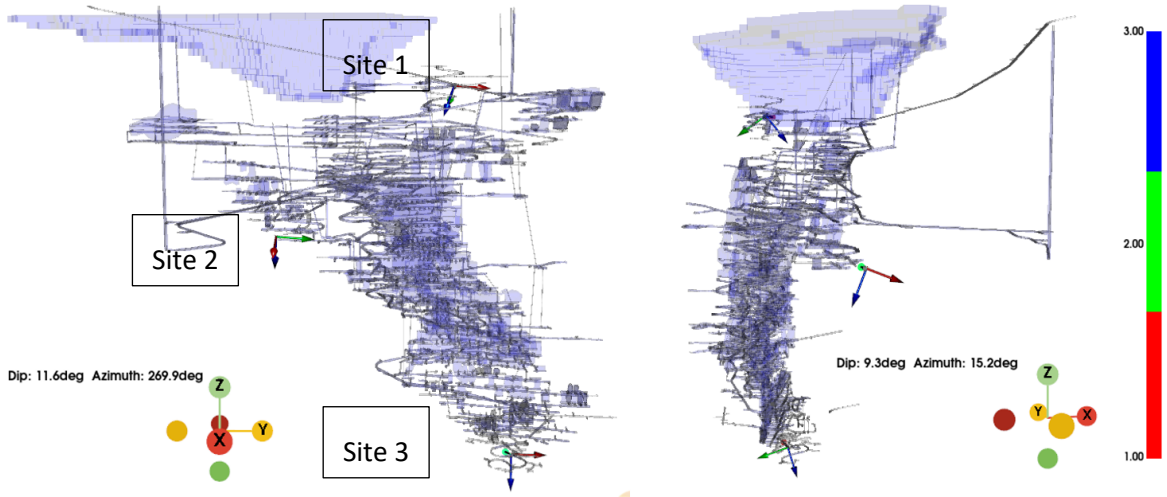

Figure 5 Measured stress orientations overlaid on the plan looking west (left) and looking north (right)

The major, intermediate and minor stress orientations were plotted on a 3D mine plan (Figure 5). The view from the west appears on the left side and the northward isometric view is on the right side. A correlation in stress orientation exists between Sites 1 and 3, where the major principal stress (red arrows) is oriented along the strike of the orebody, and the minor principal stress (blue arrows) is oriented approximately vertically. At Site 2 the major principal stress is perpendicular and the minor principal stress is vertical to the orebody.

A scatter plot depicting the measured stress versus the depth below surface is depicted in Figure 6. As expected, the stress magnitude increases with depth. However, the stresses recorded at Site 2 were significantly higher than expected from interpolation and the measurements there were discarded. It was also thought that the stress values at Site 1 were higher than predicted for an isolated test site and this was confirmed by an empirical calculation and running a numerical model using the pre-Y2023 stress state. It was concluded that the stresses at Site 1 should also be disregarded because if the stress measurements (considering Site 1 and 3) are extrapolated to the ground surface, the value of the overburden stress at the ground surface would be 14 MPa. A possible explanation could be that Site 1 was not as isolated from stress interaction with other excavations as was thought when the stress measurement plan was developed.

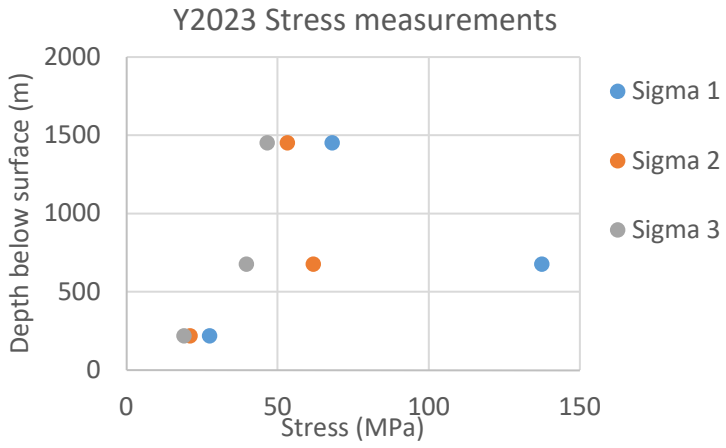

Figure 6 Measured stress magnitudes versus depth below surface

It was decided that the stress state depicted in Figure 7 should be used for future designs because:

- Directions of the pre-Y2023 stresses tensor were estimated from observations while for the Y2023 stress model, the magnitudes and directions were quantified.

- The pre-Y2023 stress model indicated lower stress values (relative to rock mass strength) at the planned mining depths while overstressed responses were being observed. The higher stress values (Y2023 model) provided a margin of safety in designs and the mine owner is risk adverse.

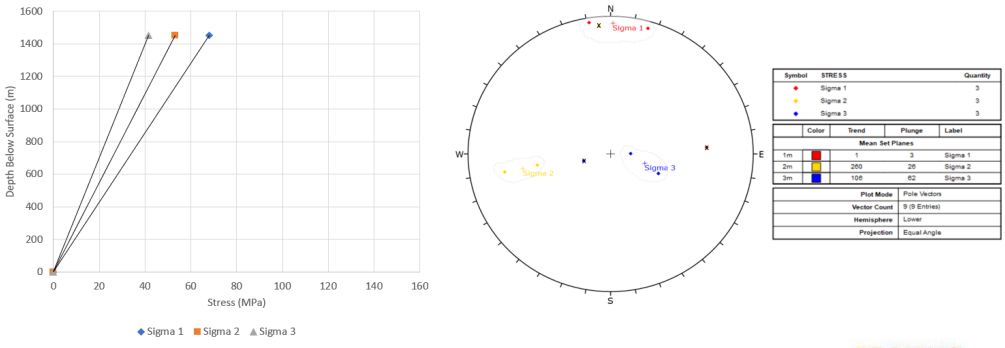

Figure 7 Stress tensor for use in subsequent modelling and analyses

3.3 Damage observations

This section contains a description of the damage observations made at Caraiba mine.

3.3.1 Unplanned sloughing

Figure 8 shows the assessed unplanned overbreak for stopes in the deeper part of the mine as the chosen stoping region is in proximity of future capital projects. The depth of overbreak ranged between 0.1 and 1.1 m, and overbreak was calculated using cavity mine surveys (CMS). After due consideration of the stope reconciliation reports it was concluded that overbreak was connected to overstressing.

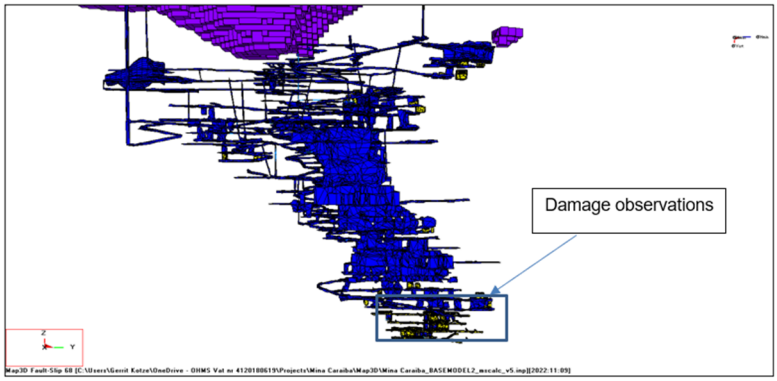

Figure 8 Mine-wide view of the Map3D model in relation to damage observations

Figure 9 depicts the design shapes used in the numerical model calibration. The labels indicate the model steps.

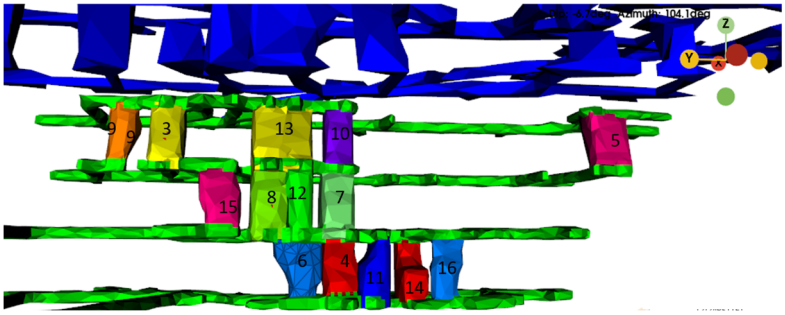

Figure 9 Zoom-in of the area where model calibration was undertaken

3.3.2 Rockburst damage

Figure 10 contains the as-built layout in the proximity of a rockburst. A middling pillar between the –500 and –520 mL galleries was planned with a 14.5 m thickness, but the as-built pillar thickness ranged from 7 to 11 m. The deviation resulted from offline mining and a change in ground conditions, which relates to a stress-induced overbreak in the hanging wall and footwall of the galleries caused by the sub-horizontal-orientated field stress.

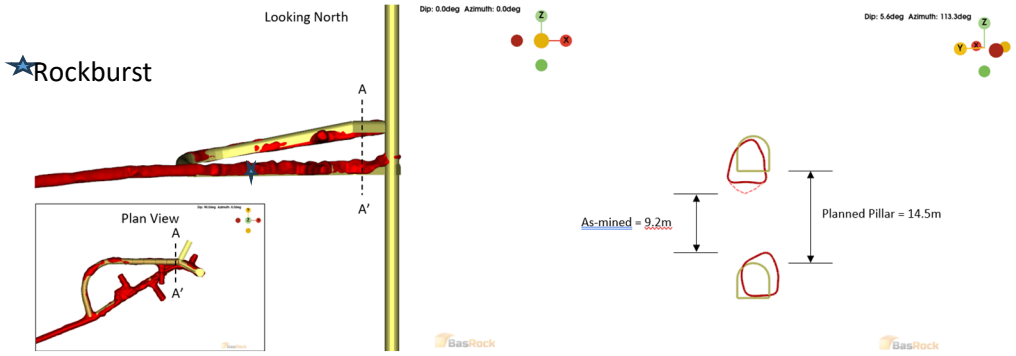

Figure 10 (a) Iso view of the geometry of the middling pillar between galleries; (b) Section view A-A')

In Figure 11 the three photographs depict damage observed in proximity to the middling pillar (at section A-A') following a flurry of seismic events. The indentation in the backs is referred to as 'Gothic arching' and is consistent with overstressing, when the major principal stress is orientated sub-horizontally and acting in a near-normal orientation to the gallery.

Figure 11 Rockburst damage: (a) Shakedown; (b) Hanging wall damage; (c) Footwall heave

Before interpretation of the rock mass response relative to the orientation of field stresses could be done it was important to determine the potential of the rock being overstressed locally and that damage was not triggered by a remotely located seismic source. Therefore a back-analysis of the largest magnitude seismic event, of local magnitude (ML) 1.7, and the flurry of seismicity, which occurred in proximity of the middling pillar, was conducted. Based on the location, fragmentation and size of the area covered in debris it was concluded that the seismic source had to be in proximity of the gallery as opposed to a remote event that induced local falls of ground. Subsequently the logarithm of the energy_S-wave to energy_P-wave ratio, or log (Es/Ep) ratio, of the largest event (ML = 1.7) was considered. The value of this ratio was 0.5 and is consistent with the range for burst-type events. Discontinuities such as persistent joints, shear structures or faults, which pierce the galleries, did not present evidence of fresh displacement that would occur during a dynamic event and were therefore eliminated as potential sources of seismic events. The source analyses on those events were not pursued further.

Using the equation proposed by McGarr & Wiebols (1977), an estimate was made of the seismic moment for a pillar which failed along a maximum length of 20 m at a thickness of 9 m. The seismic moment can be related to moment magnitude using the equations proposed by Hanks & Kanamori (1979). From the estimates it was found that the anticipated maximum event magnitude was in the range of 1.6 to 2.0. Although on different scales there was a reasonable agreement between the expected event magnitude and actual event magnitude of ML1.7, originating from the pillarburst.

Following the seismic source analyses the likely field stress orientation was assessed considering the borehole spalling (dog-earing) in a nearby vertical borehole located at a significant stand-off to open stopes but in proximity of the pillar. Figure 12 is used to depict the rose diagrams prepared for the breakout analyses and the stress orientation, which were overlaid on a plan view of the area of interest.

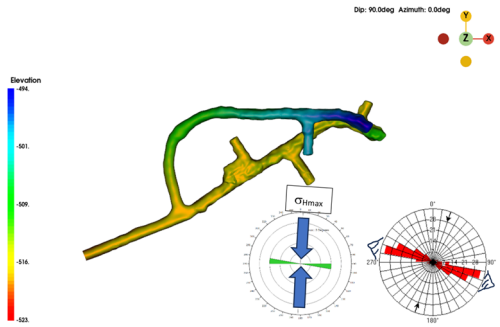

Figure 12 Rose diagrams to illustrate borehole break (red) and orientation of stress (green)

The rose diagrams were drafted in the conventional manner and annotation was added to aid in the explanation. The rose diagram in the bottom middle corner (green bars) is used to represent the measured (Y2023) maximum horizontal, pre-mining stress orientation. As per convention, the green bars are indicated on the diagram, normal to this direction. It is expected that the pre-mining stress will be oriented marginally differently compared to the horizontal field stress in the area of interest. This discrepancy arises because the galleries are expected to interact from a stress perspective to some extent. Nevertheless, the green bars give a reasonable orientation of field stress in the plane of the analyses. The representation on the rose diagram on the bottom right (red bars) corresponds to alignment of the indentations from spalling that will form when the major horizontal principal (field) stress is acting normally (plan view) to the vertical borehole. The red bars represent over 45 measurements obtained with wireline logging.

In summary, considering the impression of spalling in the backs of galleries (Figure 11) and the borehole spalling indentations (Figure 12), the field stress orientation could be inferred with reasonable confidence around the rockburst location. Hence it was concluded that the middling pillar likely experienced overstressing in a direction near-normal to its long axis, spanning a distance of 20 m. The dimension critical for stability of the pillar was therefore thought to be overloaded by stress and acting subnormally to the pillar's long axis. The reduction in pillar geometry was not conducive to stable crushing of the pillar. Evidence from various studies, including those conducted at South African platinum mines (Conbulat et al. 2006; Lunder & Pakalnis 1997), suggests that pillar yield occurs when pillar strength is exceeded on a pillar with a width to height ratio less than 2.5.

The pre-Y2023 stress measurements indicated a major horizontal stress orientation subparallel to the long axis of the middling pillar. An unlikely interpretation of the rockburst would be that that overstressing of the pillar occurred in the direction where it is geometrically strongest. Upon analysing all available observations and source mechanisms it was therefore concluded that the ML1.7 rockburst was consistent with the interpretation that the middling pillar failed. The back-analyses provided confidence in the orientation of the major principal field stress (Y2023), i.e. subnormal to the orebody.

3.3.3 Spalling of an orepass

Figure 13 shows an isometric view of a 5.5 m diameter orepass that was developed for a capital expansion project at Caraiba mine. The heatmap represents the depth of overbreak. During development the orepass was routinely inspected, and it was found that considerable breakout was localised and progressing towards the intersection with a crusher chamber. The increasing depth of overbreak is consistent with the orepass experiencing an induced stress in proximity of a crusher chamber but this should be investigated further. A maximum overbreak of around 1.5 m was observed and the observations of overbreak presented an opportunity for validation of the Y2023 stress magnitudes and directions.

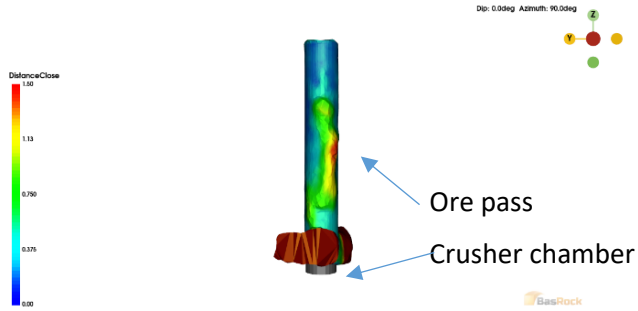

Figure 13 Isometric view of the overbreak looking east

Figure 14 illustrates various sections, spaced 3 m apart, along the length of the orepass. Refer to the plan view (right panel). Connecting the indentations from the breakout across the excavation results in a line oriented in a northeast to southwest direction. The major field stress acting on the orepass in the horizontal plane is therefore expected to align with a southeastern and northwestern direction. This direction is marginally different from the pre-mining stress direction and most likely a result of the induced stress caused by the nearby crusher chamber. Notably, a waste rock pass was experiencing breakouts as well and a similar conclusion about orientation of field stress was made.

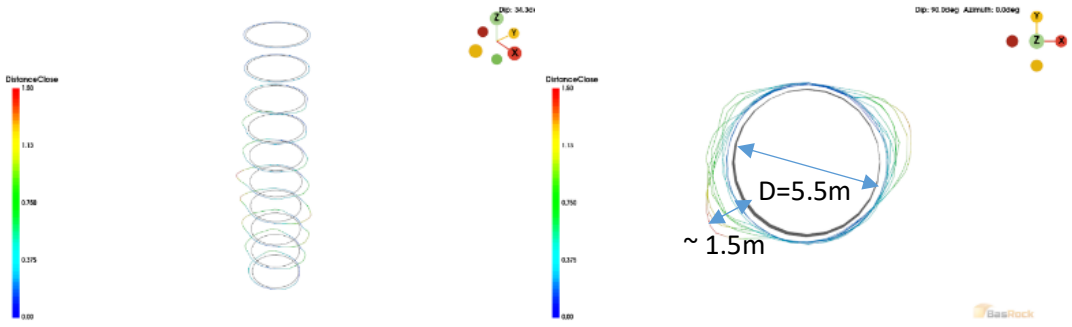

Figure 14 (a) Isometric view; (b) Plan view of orepass 1

Using the methodology proposed by Diederichs & Martin (2010), the modelled tangential stress at the location of the overbreak could be compared against expected ranges. The approach involves a graph (Figure 15) relating spalling depth to the ratio of tangential stress to UCS. For this case the suggested ratio by Diederichs & Martin (2010) is approximately 0.85. With a known UCS of 160 MPa for the gneiss host rock, the empirically established graph indicates that a tangential stress of 136 MPa (ranging between 112 MPa and 144 MPa) corresponds to a 1.5 m depth of overbreak.

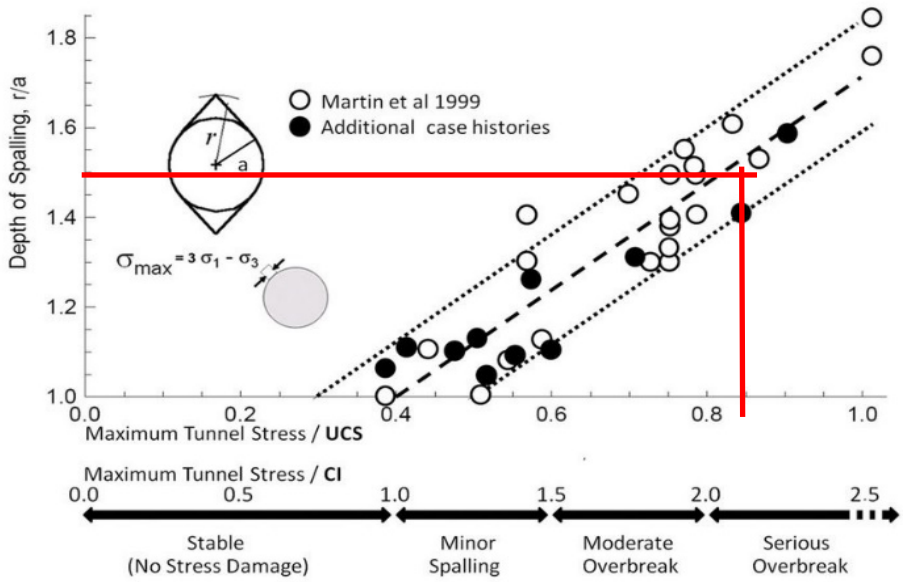

Figure 15 Depth of spalling versus stress-to-strength ratio (Diederichs & Martin 2010)

Additionally, a Map3D model (Figure 16) indicates a maximum tangential stress of 130 MPa, which falls within the same range as the empirically established value of around 136 MPa. The maximum tangential stress contours also correspond spatially with the indentations. This alignment between empirical and numerical results reflects positively on the reliability of the Y2023 stress measurements used as input parameters. This assessment provided a validation of the orientation and magnitude of the stress used as input parameters in numerical models.

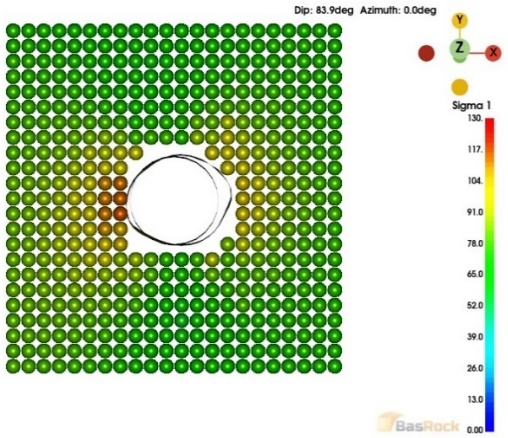

Figure 16 Plan view of field stress points depicting tangential stress in MPa, around the orepass perimeter

4 Results

The model calibration and verification process were described in Sections 2 and 3. This section outlines the results obtained. Initially the model calibration was based on a pre-Y2023 stress model and informed by field stresses collected from sloughed zones around stopes located at around 800 mbs. Subsequently the calibration was updated using the Y2023 stress measurements and the same set of stopes was assessed.

The graph depicting the initial model calibration is in Figure 17. Note that the numbers next to the symbols represent the mining step number. Model calibration is a curve-fitting exercise and regression or inspection can be used to conduct the line fit.

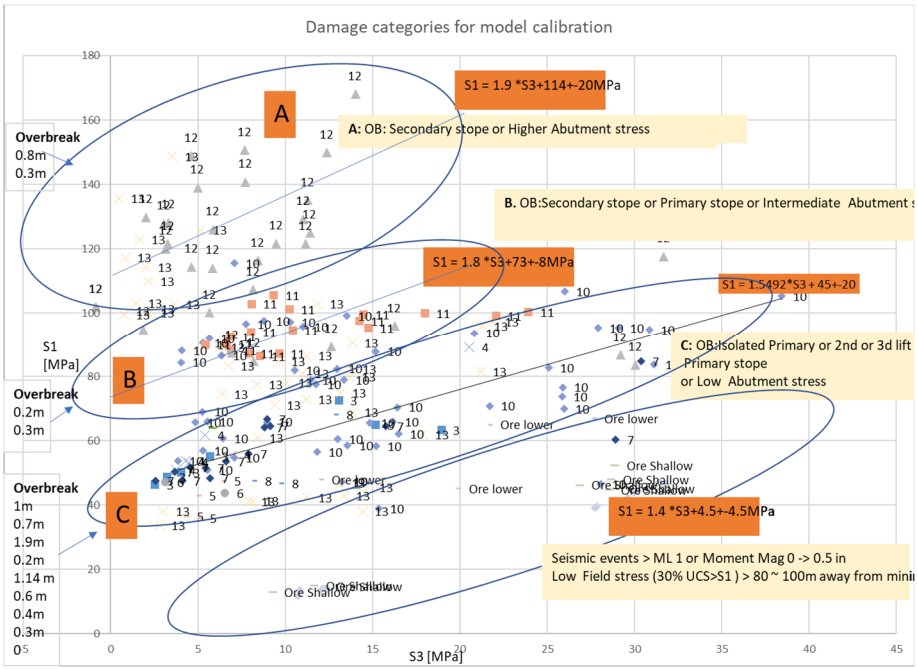

Figure 17 σ_1 (S1) versus σ_3 (S3) plot of the 2022 calibration (Kotze 2022)

The line fit was done through the centroid of the data with a view to ensuring that the slope of the fit is ≥1. In addition, as per Wiles (2024a) an attempt was made to fix the intercept at the centroid of the σ_1 data in proximity of the y-axis. Three clusters of collected σ_1 and σ_3 values associated with overbreak are found on the scatter plot. Through inspection the clusters were associated with three distinct stoping configurations, namely:

- Category A – secondary stopes or high abutment stress σ_1 ~ > 55% of UCS of gneiss and ore.
- Category B – σ_1 ~40% and 50% of UCS of gneiss and ore. The data contained in the cluster were collected from a primary stope or secondary stope, or in proximity of an abutment.
- Category C – σ_1 ~ between ~25% and 40% of UCS of gneiss and ore. The data contained in the cluster were collected from an isolated primary stope, or second or third lift primary stope, or in proximity to an abutment. The data in this cluster is from steps 3 to 10, 12 and 13.

A fourth dataset, representing principal stress pairs collected at seismic event locations (ML > 1), was also considered for model calibration. However, the seismic events were located in low-stress zones at a significant stand-off from stoping excavations. Thus from first principles and considering that the velocity model has not been calibrated for the seismic system, the locations are questionable. Seismicity was therefore excluded in this round of model calibration.

The lower boundary stress envelope for the onset of potential stress-induced overbreak is represented by Equation 4, i.e. Category C:

$$S1_{threshold} = (1.5492 \times S3 + 45 \pm 20) \quad (4)$$

where:

S1 = sigma 1 or σ_1, major principal stress.

S3 = sigma 3 or σ_3, minor principal stress.

Equation 4 represents a conservative approach to calibration for the early warning of conditions consistent with potential overbreak. After obtaining the Y2023 stress measurements (Section 3.2.) the same Map3D model was run again, and σ_1 and σ_3 values were collected at the same positions as those in the 2022 study (Kotze 2022). The calibration graph was reproduced and is depicted in Figure 18. Note that Category A was

excluded as it contained only two case studies. The dataset consistent with Category A will be developed in the future. The label numbers refer to the mining step in the model.

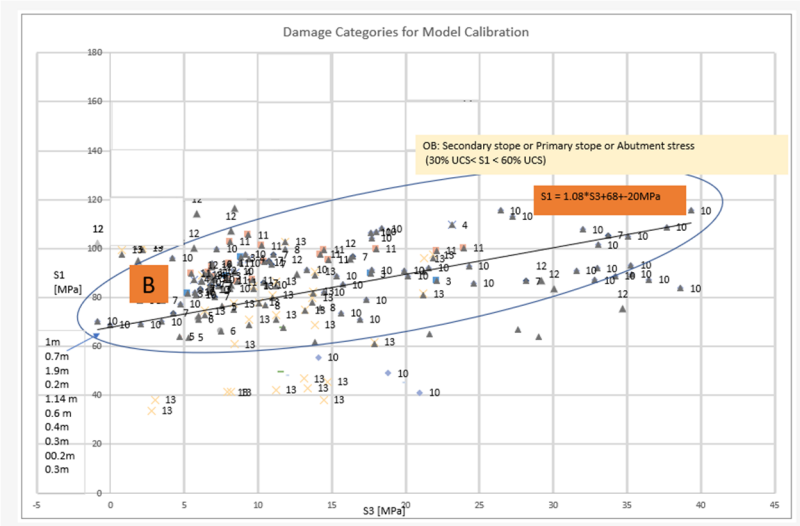

Figure 18 Updated model calibration, S1 versus S3 plot for Category B to estimate sloughing

From the graph it is evident that Categories B and C merged, and the latter cluster shifted to higher stress ranges. This observation aligns with the observed increase in magnitude and the orientation of pre-mining stress (Y2023 model). The updated Category B represents secondary stopes, primary stopes or abutments. The updated strength relation takes the form of:

$$S1_{threshold} = (1.08 \times S3 + 68 \pm 20) \quad (5)$$

where:

S1 = sigma 1 or σ_1, major principal stress.

S3 = sigma 3 or σ_3, minor principal stress.

As a result of the shift in the scatter plot due to recalibration, the descriptive statistics were updated for Category B. Table 3 contains the descriptive statistical parameters for the latest calibration (Y2023 stress model) versus the initial calibration (pre-Y2023 stress model) The results are presented in terms of S1 because, as an initial approach to interpret overbreak, the increase in stope face loading was due to the major principal stress (refer to Figure 1, left panel) as a potential mechanism for explaining stress-induced sloughing. In such an approach, the Excel function STEYX is used as a proxy for standard deviation. STEYX considers the variation in σ_1 parallel to the y-axis on a scatter plot, unlike the standard deviation, which is perpendicular to a regression line. STEYX is used with the average to calculate the coefficient of variation (CoV) in view of expressing reliability (Harr 1987).

Table 3 Updated versus previous descriptive statistical parameters for σ_1, Category B

	Initial descriptive statistical parameters (pre-Y2023 stress)	Updated descriptive statistical parameters (Y2023 stress)
Number of observations	80	143
Skewness	0.0	0.0
Standard deviation (STEYX)	12.1 MPa	12.5 MPa
Average	56.5 MPa	88.2 MPa
Coefficient of variation	0.21	0.14

The skewness of 0 indicates a normal distribution of σ_1. The initial calibration has a CoV of 21%, which is less than the acceptance criteria of 30% suggested by Wiles (2005). The interpretation of this result suggests that the initial calibration requires optimisation due to the questionable reliability of input parameters. The updated calibration has a CoV of 14%, which is in the range of the 30% suggested by Wiles (2005) and, considering only statistics, suggests a more reliable calibration (Harr 1987) due to the smaller scatter of data around the average. The updated strength envelopes and rock mass strength parameters are tabulated in Table 4.

Table 4 Updated model calibration parameters

Category	Description of stresses based on range of S1 relative to UCS	Equation	q (slope of trend line)	Friction angle (degrees)	UCS of the rock mass (MPa)	Cohesion based on mean UCS (MPa)
B	30% < S1 < 60% of UCS of gneiss and ore	S1 = 1.08 * S3 + 68 ± 20 MPa	1.08	17	68 ± 20 MPa	25 MPa

5 Conclusion

A workflow for model calibration which is intuitive and easy to routinely implement on a operational basis was discussed. Initially the model's strength envelope calibration was based on damage observations and an anecdotal stress model. After recording more stress measurements, a recalibration was made and validated against a range of rock mass responses. Despite the improved results on statistical grounds (CoV), caution should be maintained. The recalibrated strength envelope has a wider range around the mean but the mean σ_1 is higher, resulting in a lower CoV for the recalibration.

Some of the unaccounted factors potentially influencing the baseline CoV of the model calibration are:

- the model geometry when simplified for the purposes of the numerical model convergence
- the numerical model error
- the fact that one accepted stress measurement was used in the Y2023 stress model.

Other refinements to the model calibration under consideration are the potentially less-apparent influencers (relative to stress) of overbreak: geology, local variation in rock mass quality parameters, the possibility that the yielded zone extended beyond the limits of the CMS and data selection biases in models.

Notably, this CoV falls within the range indicated by Wiles (2005) and is of the same order (approximately 20% to 30%) as the CoV observed in laboratory tests (Harr 1978). It is encouraging that the enhanced reliability was achieved through the combination of a quantified stress state as a model input and empirical data. These results suggest that elastic modelling suffices for model calibration, back-analyses and predictions in this specific geotechnical setting, and that reliability may possibly be improved by adding more cases. Continuous improvement of the quantity and quality of data would bolster confidence in the input data used for calibration. Until more cases are added, and the reliability assessed again, plastic modelling is not feasible as the full advantages of minimal input parameters and intuitive model calibration methods have not yet been fully harnessed.

6 Acknowledgement

The authors thank the mine management of Ero Copper Corporation's Caraiba mine for permission to publish this material. They also express gratitude towards the mining geotechnical engineering consultants at Open House Management Solutions for allowing their senior consultants to allocate time for this paper to be written.

References

Castro, LAM 1996, *Analysis of Stress-Induced Damage Initiation around Deep Openings Excavated in a Moderately Jointed Brittle Rock Mass*, PhD thesis, University of Toronto, Toronto.

Conbulat, I, Grodner, M, Lightfoot, N, Ryder, J, Essrich, F, Dlokweni, T & Prohaska, G 2006, *The Determination of Loading Conditions for Crush Pillars and the Performance of Crush Pillars Under Dynamic Loading*, Safety in Mines Research Advisory Committee, Johannesburg.

Diederichs, MS & Martin, CD 2010, 'Measurement of spalling parameters from laboratory testing', *Rock Mechanics in Civil and Environmental Engineering*, 1st edn, CRC Press, Boca Raton.

Diederichs, M.S., Kaiser, P.K. & Eberhardt, E. 2004, 'Damage initiation and propagation in hard rock during tunnelling and the influence of near-face stress rotation', *International Journal of Rock Mechanics and Mining Sciences*, vol. 41, no. 5, pp. 785–812.

Ero Copper Corporation 2022, *Mineral Resources and Mineral Reserves of the Caraíba Operations, Curaçá Valley, Bahia, Brazil*, Ero Copper, Vancouver.

Hanks, TC & Kanamori, H 1979, 'A moment magnitude scale', *Journal of Geophysical Research*, vol. 84, no. B5, pp 2348–2350.

Harr, ME 1978, 'Elements of probability', *Reliability-Based Design in Civil Engineering*, McGraw-Hill Book Company, New York, pp. 21–31.

Kotze, G 2022, *Initial Numerical Modelling-Based Assessment of the As-Built, Planned Mining of Year 2023/2024 and the Planned Shaft Infrastructure Expansion*, unpublished report to the client, Potchefstroom.

Lunder, PJ & Pakalnis, R 1997, 'Determination of the strength of hardrock mine pillars', *Bulletin of the Canadian Institute of Mining and Metallurgy*, vol. 90, pp. 51–55.

McGarr, A & Wiebols, GA 1977, 'Influence of mine geometry and closure volume on seismicity in a deep level mine', *International Journal of Rock Mechanics and Mining Sciences and Geomechanics Abstracts*, vol. 14, pp. 139–145.

Martin, CD 1997, 'Seventeenth Canadian geotechnical colloquium: the effect of cohesion loss and stress path on brittle rock strength', *Canadian Geotechnical Journal*, vol. 34, no. 5, pp. 698–725.

Martin, CD & Maybee, WG 2000, 'The strength of hard rock pillars', *International Journal of Rock Mechanics and Mining Sciences*, vol. 37, pp. 1239–1246.

Simms, C 2024, *What is Occam's Razor?*, New Scientist, London, viewed 9 July 2024, https://www.newscientist.com/definition/occams-razor

Wiles, TD 2005, 'Reliability of numerical modelling predictions', *International Journal of Rock Mechanics and Mining Sciences*, vol. 43, no. 3, pp. 1239–1246.

Wiles, TD 2024a, *Map3D Course Notes: KB Example*, Map3D International (Pty) Ltd., Toronto, viewed 17 April 2024, www.map3d.com/download

Wiles, TD 2024b, *Map3D User's Manual*, Mine modelling (Pty), Canada.